


SCIENTIFIC REPORTS



OPEN

CoCO₃ from one-step micro-emulsion method as electrode materials for Faradaic capacitors

Yanfang Wang^{1,2}, Zheng Chang², Yi Zhang¹, Bingwei Chen², Lijun Fu¹, Yusong Zhu¹, Lixin Zhang² & Yuping Wu^{1,2} 

Faradaic capacitor (FC) has been widely investigated during the past few decades, and dozens of prototypes have been proposed. However, it has not reached its full potential. In this work, we demonstrate a kind of FC comprising of a CoCO₃ electrode. Synthesized through a micro-emulsion route, such CoCO₃ shows low crystallinity and porous wool-ball structures stacked by needle-like individuals. It shows desirable electrochemical properties in terms of excellent high-rate performance and high reversibility. Also, it could deliver a capacitance of 440 F·g⁻¹ at 1 A·g⁻¹, and shows no capacitance decay after 1000 cycles. Since metal carbonate is capable of delivering good electrochemical performances and its preparation is easier and more cost-efficient, it should be a feasible candidate for electrode material of FC.

With the highly increasing demands for energy consumption, various alternative energy sources having attractive features have come into researchers' sights. Among them, secondary energy resources such as wind and solar energy are thought to be the most appealing candidates thanks to their renewability and cleanliness. However, harnessing energy from such sources is not always conceivable because various factors like location and climate could influence this process¹. Scientists having different backgrounds and specialties, in order to better the utilization of these changeable energy resources, have demonstrated storing such intermittent energy in electrical energy storage (EES) devices to be a feasible solution. During the past decades, dozens of EES devices such as M-ion batteries (M = Li, Na and Al)²⁻⁵, metal-air batteries⁶⁻⁸, metal-sulfur batteries⁹⁻¹², redox flow batteries and supercapacitors¹³⁻¹⁵ have been reported.

Electrochemical capacitor (EC), also called as supercapacitor, has drawn special attentions thanks to its fascinating properties, e.g. fast response, durable cycling ability and high power density¹⁶. Typically, there are two types of ECs which are classified according to their working mechanisms, i.e. electrochemical double-layer capacitor (EDLC) and Faradaic capacitor (FC, or battery-type capacitor)¹⁷. For EDLCs, the electrode materials usually are porous carbons having no electrochemical activity. In other words, only physical charge accumulation occurs at the electrode/electrolyte interface during the charge and discharge processes. For Faradaic capacitor (FC) or pseudocapacitor, charge storage and release are always accompanied by fast and reversible reactions happening on the surface or in near-surface areas. In this case, the electrode materials are electrochemically active. Generally, due to their different mechanisms, the EDLCs display higher rate capability and better cycling stability, but lower specific capacitance and energy density than those of the FCs. Trying to praise one more than the other is unreasonable, and it is clear that both of them have not reached their full potentials.

Hitherto, various materials such as transition metal oxides, metal hydroxides and conductive polymers have been investigated as electrode materials for FCs¹⁸. Taking Co₃O₄ as an example, in order to fabricate effective structures, various ways such as template-method, hydrothermal method and electrochemical deposition were explored¹⁹⁻²¹. However, such methods usually involve at least two steps. One is the preparation for precursors such as Co(OH)₂. Following is the conversion process from precursors to final products, in which calcination is needed and more energy is consumed. In fact, the extra energy could be saved by leaving out of the thermal

¹School of Energy Science and Engineering & Institute for Electrochemical Energy Storage, Nanjing Tech University, Nanjing, 211816, China. ²New Energy and Materials Laboratory (NEML), Department of Chemistry and Shanghai Key Laboratory of Molecular Catalysis and Innovative Materials, Fudan University, Shanghai, 200433, China. Correspondence and requests for materials should be addressed to L.F. (email: l.fu@njtech.edu.cn) or Y.Z. (email: zhuy@njtech.edu.cn) or Y.W. (email: wuyup@fudan.edu.cn)

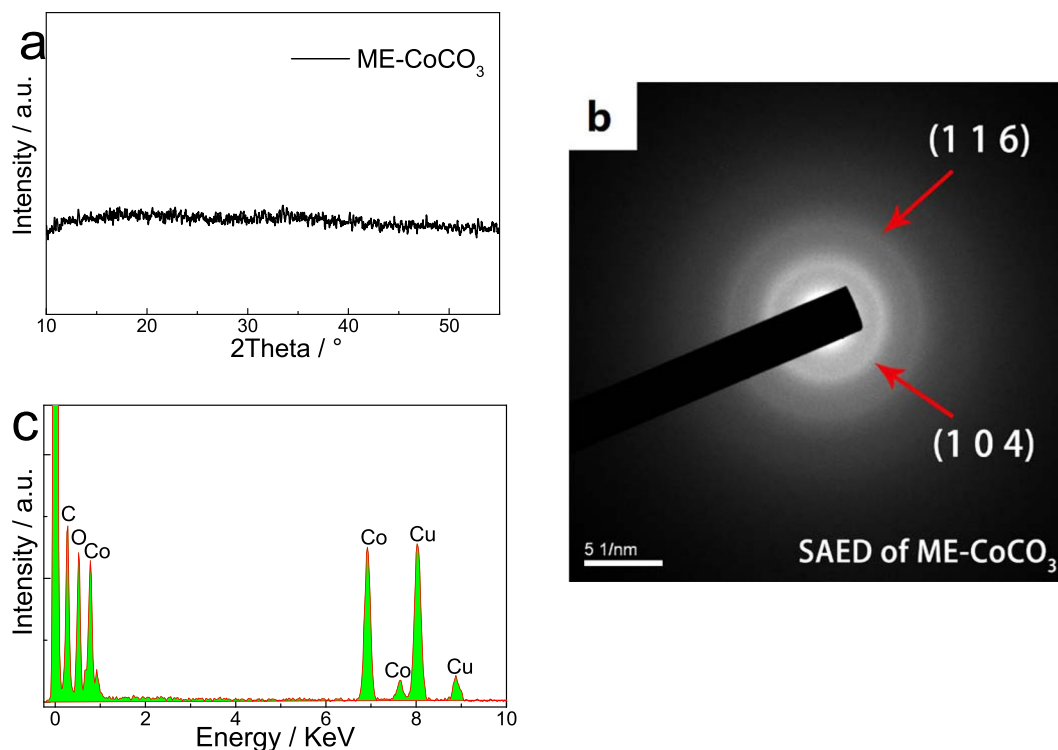


Figure 1. Some physical properties of the prepared ME-CoCO₃: (a) XRD patterns (b) selected area electron diffraction (SAED) micrograph, and (c) energy dispersive X-ray spectroscopy (EDX) analyses.

treatment. Actually, during the past few years, calcination-free Co(OH)₂ has attracted widely research interests since it could be prepared in more cost-effective routes and is able to deliver good performances^{22–26}.

Herein, inspired by the success of Co(OH)₂, we have tried to demonstrate the possibility of fabricating FCs by using CoCO₃ electrodes, and it ends up to be a good attempt. In this work, a kind of “wool-ball” like CoCO₃ possessing amorphous and porous structure has been synthesized by using a soft template method based on reverse micelles. When being tested as electrode for FC in aqueous alkaline solution (0.5 M KOH), it could deliver a reversible specific capacitance of more than 400 F·g⁻¹ as well as a 100% capacitance retention after 1000 cycles (at the current density of 1 A·g⁻¹). The reaction intermediates appearing in the charge-discharge processes have been well studied and the reaction mechanisms have been expounded and proved. The results of our study on CoCO₃, to some extent, could be analogized to other metal carbonates such as MnCO₃ and NiCO₃.

Results

Determined by the calcination-free routes, the X-ray diffraction patterns of the sample show dispersed diffraction peaks, demonstrating that it has low crystallinity (Fig. 1a). Two diffused halo rings observed in the selected area electron diffraction (SAED) patterns, which can be indexed to (104) and (116) planes of CoCO₃ (JPCDS 11-0692), also verify its low crystallinity (Fig. 1b). Materials having low crystallinities always need lower energy and show higher rate performance when going through chemical reactions since phase transformation is always accompanied by crystal conversion, but such process is not necessary for amorphous materials. As shown in Fig. 1c, the atomic ratio of Co and O is calculated to be 1:2.71 based on the results of energy dispersive X-ray spectroscopy (EDX). Besides, the as prepared CoCO₃ was tested by using a thermogravimetric-mass spectrum (TG-MS) combined system (Figure S1). As shown in the TG curve, there is 10% weight loss as the temperature increases to 175 °C. The signal of CO₂ (m/z = 44) shows a peak in the region of 75–175 °C, which means that CoCO₃ begins to decompose. Then, a sharp weight loss appears beginning at 200 °C, and it is accompanied by the release of large amounts of CO₂ (the strong peak at around 275 °C in the mass spectra). The total weight loss is about 35%, which is consistent with the decomposition of CoCO₃ into CoO. Thus, the sample is mainly consisted of CoCO₃. If xCoCO₃·yCo(OH)₂·zH₂O exists, its amount is very small.

Figure 2a and b show scanning electron microscopy (SEM) micrographs of CoCO₃ samples synthesized through micro-emulsion (ME-CoCO₃) and co-precipitation routes (CP-CoCO₃), respectively. Both of them are nanoparticles with sizes of 100–500 nm. Specially, the ME-CoCO₃ exhibits some uncommon surface structures which could be formed with the help of surfactants. As shown in the transmission electron microscopy (TEM) micrograph (Fig. 2c and Figure S2), the special surface structures could be determined to be needle-like CoCO₃ individuals, which then accumulated to form “wool-ball” like nanoparticles. Since these individuals cannot stack compactly, CoCO₃ nanoparticles tend to develop into porous structures, which could be confirmed by the enlarged TEM micrograph (Fig. 2d). Commonly, materials for FCs suffer from inevitable volumetric expansions during the charge and discharge processes, which then result in fast capacitance decline. Therefore,

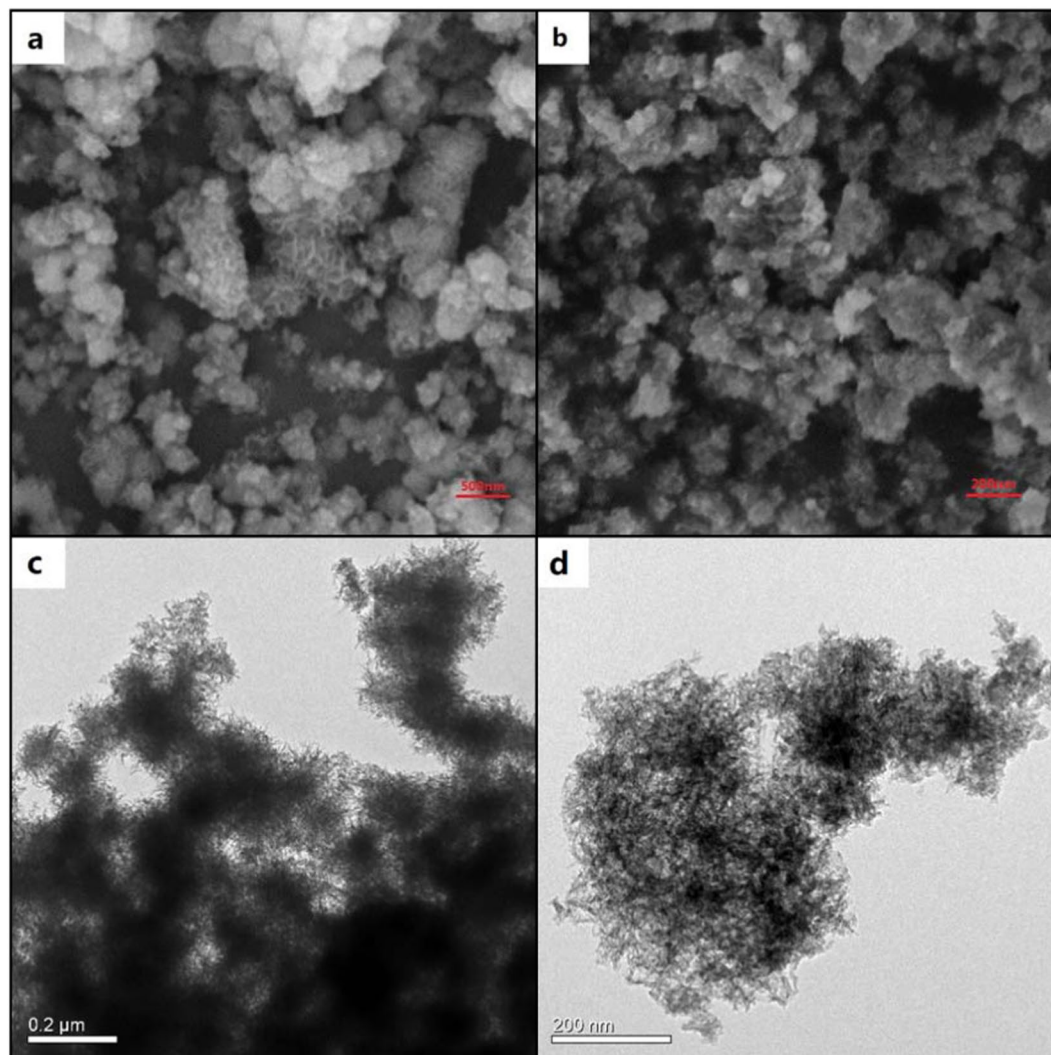


Figure 2. SEM micrographs of (a) ME-CoCO₃ and (b) CP-CoCO₃, (c) low and (d) high magnification TEM micrographs of ME-CoCO₃.

possessing porous structures means that the ME-CoCO₃ could have enough space for expansion and thus could be able to have a long life span. Also, such porous structure could increase its specific surface areas which in turn could facilitate ion transfer and improve its rate performance. The nitrogen adsorption-desorption results reveal that ME-CoCO₃ has a specific surface area (S_{BET}) of $41.6 \text{ m}^2 \text{ g}^{-1}$ which is much larger than that of CP-CoCO₃ ($23.1 \text{ m}^2 \text{ g}^{-1}$). The higher specific surface area and porous structure allows it to possess larger interfaces connecting with conducting additives (acetylene black), which will lead to lower internal resistance.

Figure 3a exhibits the cyclic voltammetry (CV) curves of ME-CoCO₃. As shown, in the first cycle, two oxidation peaks centered at 0.2 and 0.48 V could be observed. Therefore, Co (II) should be oxidized to Co (IV) with an intermediate state of Co (III). In addition, the first peak has higher intensity in the first cycle, which means that large amounts of Co (II) have converted into Co (III) during this process. However, the reduction peak regarding the reaction from Co (III) to Co (II) shows much lower peak current density, demonstrating that such oxidation process (Co(II) to Co(III)) in the first cycle is irreversible. Clearly, in the second cycle, the intensity of first oxidation peak decreases sharply. Thus, the reversible reaction between Co(III) and Co(IV) dominates in the second and the following cycles.

Figure 3b shows the charge-discharge curves of ME-CoCO₃ after CV test. The specific capacitance was calculated according to the following equation:

$$C_m = I \cdot t / (\Delta V \cdot m) \quad (1)$$

where C_m is the specific capacitance of the electrode material ($\text{F} \cdot \text{g}^{-1}$), I is the charge/discharge current (A), t is the charge/discharge time (s), ΔV is the potential window, and m is the mass of electrochemical active material. A pair of plateaus could be observed in the charge-discharge curves, which are in accordance with the reversible conversion between Co(III) and Co (IV). Electrode materials were collected at the beginning of the plateau and at the end of the charge process, and were notated as state 1 and state 2, respectively. Then, such materials were

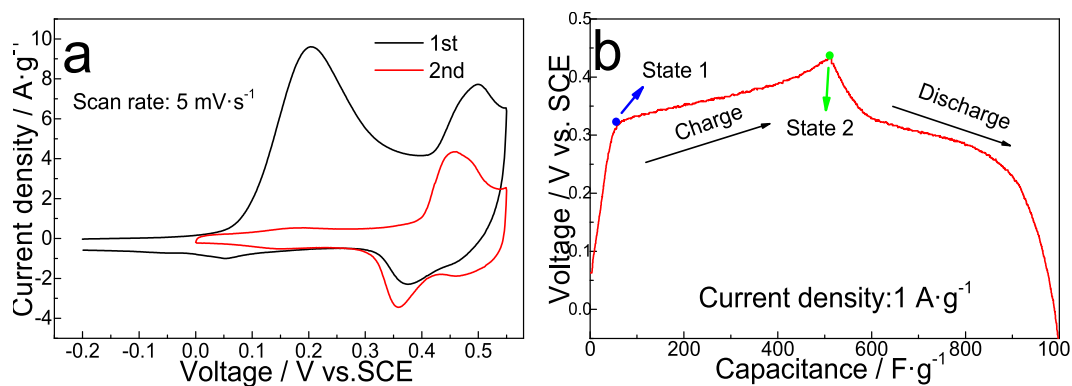


Figure 3. (a) CV curves and (b) charge-discharge curves of ME-CoCO₃.

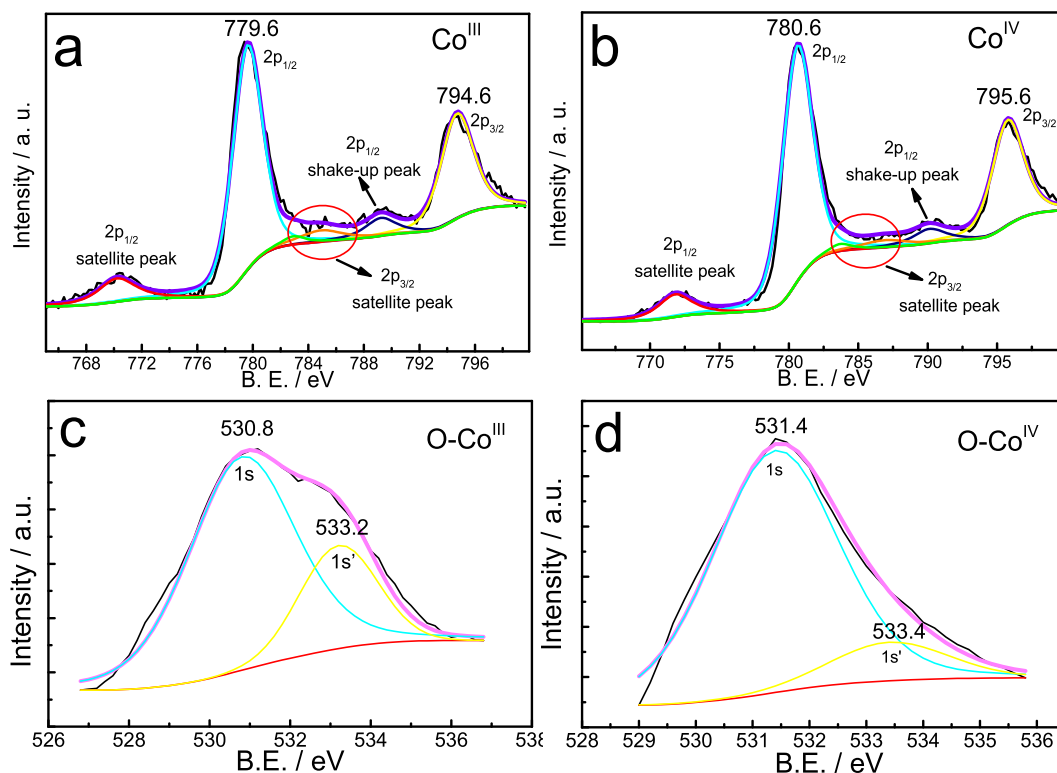
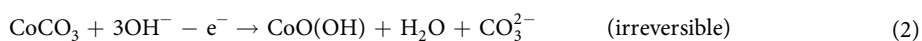


Figure 4. XPS spectra of (a) Co and (c) O at state 1 and those of (b) Co and (d) O at state 2 indicated in Fig. 3b.

characterized with XPS technique (Fig. 4). As shown in Fig. 4a, two typical peaks centered at 794.6 and 779.6 eV in the Co_{2p} spectra (Fig. 4a) are accordant with the Co_{2p_{3/2}} and Co_{2p_{1/2}} spin-orbit peaks of Co(III). In addition, there are some small peaks. The satellite peaks located at around 770 and 785 eV should be caused by some minor impurities, and the peak located at around 790 eV could be assigned to the shake-up peak of Co_{2p_{1/2}}. The split O_{1s} peaks centered at 530.8 and 533.2 eV indicate that O exists in two forms at state 1 (Fig. 4c). As for state 2, in the Co_{2p} spectra (Fig. 4b), two typical peaks centered at 795.6 and 780.6 eV could be assigned to the Co_{2p_{3/2}} and Co_{2p_{1/2}} spin-orbit peaks of Co(IV). In the O_{1s} spectra (Fig. 4d), the areas surrounded by the typical peak centered at 531.4 eV are much larger than that surrounded by the peak centered at 533.4 eV, implying that O exists in one major phase. Therefore, the main compound at state 1 and state 2 should be CoOOH and CoO₂, respectively. Besides, the small peak of O_{1s} detected at 533.4 eV corresponds to the O in H₂O.

According to the above results, the reaction mechanisms of CoCO₃ in alkaline solutions can be proposed as follows:



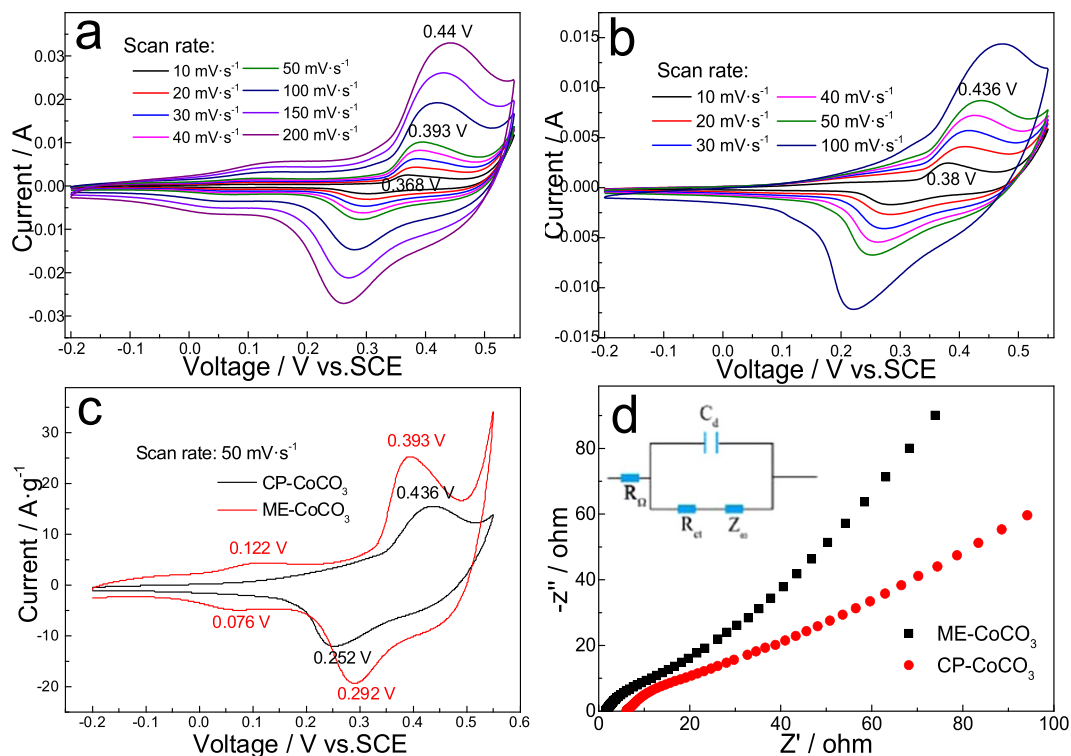
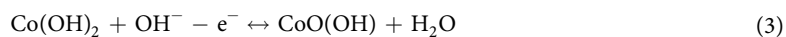


Figure 5. CV curves of (a) ME-CoCO₃, (b) CP-CoCO₃ at different scan rates and (c) both of them at the scan rate of 50 mV·s⁻¹, and (d) their EIS results.



In alkaline solutions, cobalt carbonate would convert to cobalt hydroxide spontaneously according to the precipitation and dissolution equilibrium. Such process could be speeded up by forward current since the movement of ions could be promoted under current. Therefore, CoCO₃ would convert to Co(OH)₂ and CoOOH rapidly in the 1st cycle (Equation 2), and such conversion is irreversible, which has been demonstrated by the CV curve. Then, during the following cycles, conversions between Co(OH)₂/CoOOH and CoO₂ would happen reversibly (equations 3 and 4).

Figure 5a shows the CV curves of ME-CoCO₃ at various potential scan rates. Two pairs of peaks could be seen at all scan rates, and the conversion between Co(III) and Co(IV) dominates in all cases. Specially, the CV curves maintain regular shapes even at a very high scan rate of 200 mV·s⁻¹, showing that it has excellent high-rate performance. In the case of the CP-CoCO₃, its CV curves show severe distortion with increasing scan rates (Fig. 5b). In addition, the symmetric CV curves prove that the redox reactions occurring in both electrodes are reversible.

The electrochemical impedance spectroscopy (EIS) results are shown in Fig. 5d. The internal resistance of an electrode (notated as R_{Ω} or R_{ESR}), i.e. the point intersecting with real axis at high frequency, includes ionic resistance of electrolyte (R_A), intrinsic resistance of electrode materials (R_B) and contact resistance (R_C , negligible due to the high conductivity of nickel mesh). The polarization resistance (R_p), i.e. the diameter of semicircle, reveals penetrating ability of electrolyte into porous electrode. The diffusional resistance (R_D), i.e. the length of 45° line in middle frequency region, indicates migration rate of ions from electrolyte inside pores to the electrode surface. The sum of R_D and R_p is notated as charge transfer resistance (R_{ct})²⁷. Clearly, the ME-CoCO₃ electrode presents smaller R_{ESR} (2.0 Ω) than the CP-CoCO₃ (6.3 Ω), demonstrating its better electronic conductivity. Also, the R_{ct} of the ME-CoCO₃ (15 Ω) is smaller than that of the CP-CoCO₃ (28 Ω) thanks to its “wool-ball” like structure. Commonly, in narrow pores or nonporous structures, ion could not migrate smoothly because of large diffusion drag. In our ME-CoCO₃ electrode, the porous structure piled up by needle-like individuals could provide free pathways for ions. In the low frequency range, the larger slope of the ME-CoCO₃ electrode indicates its better capacitive behaviour.

Figure 6a and b show the galvanostatic charge-discharge curves of the ME-CoCO₃ and CP-CoCO₃ at various current densities. It can be seen that the charge and discharge times are nearly the same at a certain current density, indicating their good reversibility. Their rate and cycling performances were tested and shown in Fig. 6c. The ME-CoCO₃ could deliver a capacitance of 440 F·g⁻¹ at 1 A·g⁻¹ and 260 F·g⁻¹ at 10 A·g⁻¹, which is even higher than that at 1 A·g⁻¹ in the case of the CP-CoCO₃ (155 F·g⁻¹). As to the cycling behaviour (Fig. 6d), it can be seen that the specific capacitances of both CoCO₃ gradually increase to peak values and then decrease slightly. Such

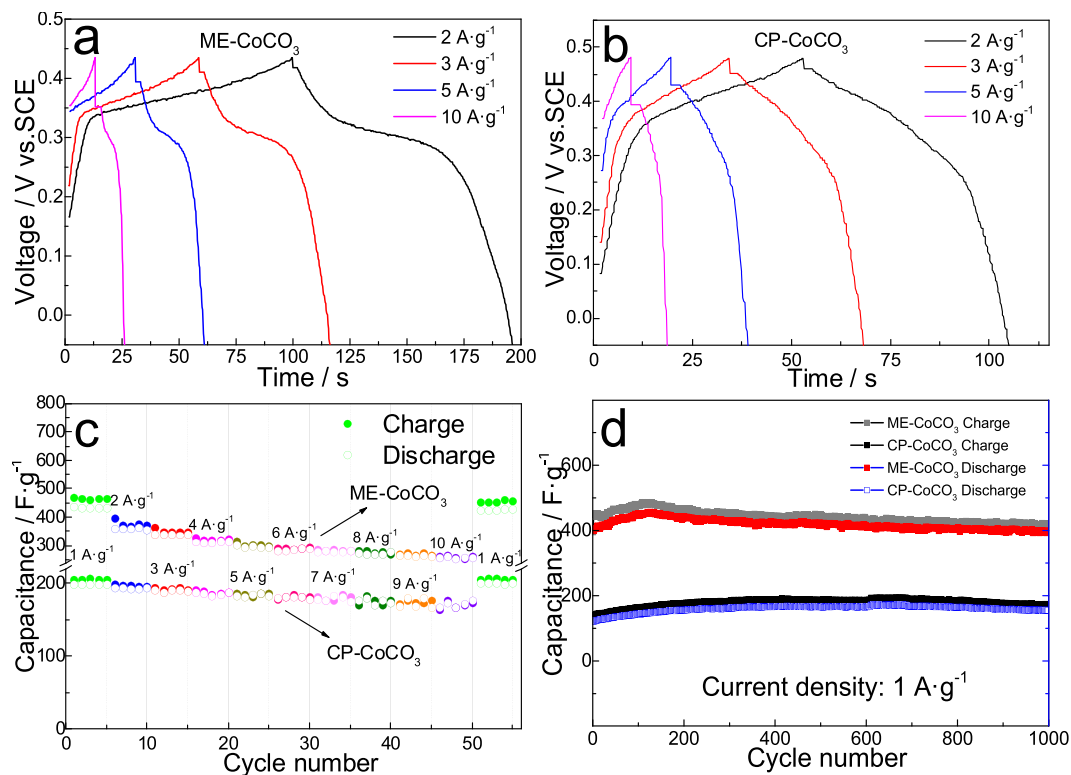


Figure 6. Galvanostatic charge-discharge curves of (a) ME-CoCO₃ and (b) CP-CoCO₃. (c) Rate performances and (d) cycling behaviours of ME-CoCO₃ and CP-CoCO₃.

increase at the initial cycling period is consistent with the activation process reported before²⁸. At the beginning of the charge/discharge processes, the electrochemical active materials could not be fully wetted by the electrolyte and only the surface areas could be utilized for charge storage, and thus the transfers of ions and electrons could not be fully realized for the electrode. Along with the continuing intercalation and de-intercalation, active sites even in the near-surface bodies could be exploited. Therefore, the capacitance could be increased and thus the electrode could reach a so-called activated state. The activation process varies with the electrode material changes. In the case of the CP-CoCO₃, the activation process lasted for 600 cycles. However, as for the ME-CoCO₃, such process only took 150 cycles thanks to its porous structure and lower R_{ct} . Then, the capacitance would decrease after reaching the ceiling value since extra stress and strain caused by volumetric expansion is inevitable in materials for FCs. Such extra stress and strain could result in structure collapse and thus reduce available active sites for charge storage. However, because of its enough space for volumetric expansion, such extra forces could not affect the ME-CoCO₃ severely. So, it shows almost no capacitance decline after 1000 cycles at 1 A·g⁻¹, which is desirable for EES applications. Figure S3 shows the long-term cycling performance of ME-CoCO₃ after activation. It could deliver 95.3% of the initial specific capacitance after 4000 cycles at 5 A·g⁻¹.

Discussion

In this report, we propose the opinion of replacing metal oxides with metal carbonates. As we demonstrate in our paper, metal carbonates could be able to perform good properties as electrodes or pre-electrodes for supercapacitors, and they could be synthesized under mild conditions such as low temperature and pressure. Here, we demonstrate a kind of FC by using CoCO₃ as electrode material and study the reaction mechanisms of CoCO₃ carefully. The synthesis of such material includes a calcination-free route, so that such energy could be saved compared with the synthesis of Co₃O₄. Besides, with the help of surfactant, CoCO₃ synthesized through micro-emulsion approach shows effective “wool-ball” like structures. Such porous structures could not only facilitate charge transfer but also provide enough space to avoid structure collapse caused by volumetric expansion. The reaction mechanisms could be explained by an irreversible conversion between Co(II) and Co(III) in the 1st cycle followed by reversible reactions. Although the reactions in the following cycles might be similar to those for Co(OH)₂ electrode, CoCO₃ is also worthy of investigation because of the possibility it offers. Not to mention that CoCO₃ would be able to meet the demands for EES devices. In the case of the ME-CoCO₃, it presents excellent high-rate performance and high reversibility. Also, it delivers a capacitance up to 440 F·g⁻¹ at 1 A·g⁻¹, and shows no capacitance decay after 1000 cycles. Therefore, CoCO₃ could be feasible candidates for FCs, and other metal carbonates such as MnCO₃ and NiCO₃ could also be available alternatives for EES applications.

Methods

Sample preparation. The CoCO_3 nanoparticles were prepared through co-precipitation routes and micro-emulsion routes^{29,30}, and they are denoted as CP- CoCO_3 and ME- CoCO_3 , respectively. In a typical process, a micro-emulsion system was first prepared by dissolving cetyltrimethyl ammonium bromide (CTAB, 4.0 g) in a mixture of cyclohexane (100 ml), *n*-pentanol (5.0 ml) and 0.1 M $(\text{NH}_4)\text{HCO}_3$ (7.5 ml) aqueous solutions. After stirring for 30 minutes, CTAB was dissolved in the solution absolutely. Then, 2.5 ml of 0.1 M $\text{Co}(\text{NO}_3)_2$ solution was added dropwise under stirring and a transparent micro-emulsion was obtained. Finally, the amaranth product was filtered, washed several times with ethanol and distilled water, and dried under 80 °C in a vacuum oven. The yield of the ME- CoCO_3 in a typical process was about 30 mg, about 80%. The CP- CoCO_3 was prepared by a co-precipitation method. An aqueous solution (25 ml of 0.1 M $\text{Co}(\text{NO}_3)_2$) was added dropwise into 30 ml 0.1 M Na_2CO_3 aqueous solutions under continuous stirring. The precipitate was collected, washed and dried under 80 °C in a vacuum oven as well.

Material characterization. X-ray diffraction (XRD) patterns were collected by using a BrukerD4 X-ray diffractometer (Bruker, Germany) with Ni-filtered $\text{Cu K}\alpha$ radiation (40 kV, 40 mA). Field emission scanning electron microscopy (FE-SEM) was performed on a FE-SEM-4800-1. Prior to the FESEM analyses, a thin layer of Au was sputtered on the surfaces of the as-prepared materials. Transmission electron microscopy (TEM) was performed by using a JEOL JEM-2010 transmission electron microscope (JEOL, Japan) operated at 200 kV. X-ray photoelectron spectroscopy (XPS) was performed by using a PHI5300 X-ray photoelectron spectroscope (Perki-Elmer, America) with aluminum target (14 kV, 250 W). Thermogravimetric-mass spectrum test was performed on SDT Q600 (USA) – GSD 301 T2 (Germany) combined system under nitrogen flow.

Electrochemical test. The as-prepared ME- CoCO_3 or CP- CoCO_3 was mixed with poly(tetrafluoroethylene) (PTFE) and acetylene black in a weight ratio of 8:1:1. The mixture was well-distributed in the ethanol with the help of ultrasonic treatment. After drying, the mixture was pressed into a film and cut into pieces. One piece with a certain mass was weighted and pressed onto a piece of nickel mesh with a mass loading of 10 mg cm^{-2} to act as the working electrode. A three-electrode system consisting of the above working electrode, nickel mesh as the counter electrode, and saturated calomel electrode (SCE) as the reference electrode was used to test the electrochemical behaviours of the electrode materials. The cyclic voltammetry (CV) measurements were tested on an electrochemical working station (CHI 440B). The charge/discharge behaviours including the rate and cycling performance were tested on a cell tester (Land, Wuhan, China).

References

- Reddy, A. L. M., Gowda, S. R., Shaijumon, M. M. & Ajayan, P. M. Hybrid nanostructures for energy storage applications. *Adv. Mater.* **24**, 5045–5064, doi:10.1002/adma.201104502 (2012).
- Hassoun, J. *et al.* An advanced lithium-ion battery based on graphene anode and a lithium iron phosphate cathode. *Nano Lett.* **14**, 4901–4906, doi:10.1021/nl502429m (2014).
- Chao, D. L. *et al.* Graphene quantum dots coated VO_2 arrays for highly durable electrodes for Li and Na ion batteries. *Nano Lett.* **15**, 565–573, doi:10.1021/nl504038s (2015).
- Tang, W. *et al.* LiMn_2O_4 nanotube as cathode material of second-level charge capability for aqueous rechargeable batteries. *Nano Lett.* **13**, 2036–2014, doi:10.1021/nl400199r (2013).
- Lin, M. C. *et al.* An ultrafast rechargeable aluminium-ion battery. *Nature* **520**, 324–328, doi:10.1038/nature14340 (2015).
- Elia, G. A. *et al.* An advanced lithium-air battery exploiting an ionic liquid-based electrolyte. *Nano Lett.* **14**, 6572–6577, doi:10.1021/nl5031985 (2014).
- Lu, Y. C. *et al.* Lithium-oxygen batteries: bridging mechanistic understanding and battery performance. *Energy Environ. Sci.* **6**, 750–768, doi:10.1039/c3ee23966g (2013).
- Bruce, P. G., Freunberger, S. A., Hardwick, L. J. & Tarascon, J. M. Li- O_2 and Li-S batteries with high energy storage. *Nat. Mater.* **11**, 19–29, doi:10.1038/nmat3191 (2012).
- Chen, L. & Shaw, L. L. Recent advances in lithium-sulfur batteries. *J. Power Sources* **267**, 770–783, doi:10.1016/j.jpowsour.2014.05.111 (2014).
- Hu, Y. Y., Wen, Z. Y., Wu, X. W. & Jin, J. Low-cost shape-control synthesis of porous carbon film on β -alumina ceramics for Na-based battery application. *J. Power Sources* **219**, 1–8, doi:10.1016/j.jpowsour.2012.07.025 (2012).
- Lalère, F. *et al.* An all-solid state NASICON sodium battery operating at 200 °C. *J. Power Sources* **247**, 975–980, doi:10.1016/j.jpowsour.2013.09.051 (2014).
- Hwang, T. H., Jung, D. S., Kim, J. S., Kim, B. G. & Choi, J. W. One-dimensional carbon-sulfur composite fibers for Na-S rechargeable batteries operating at room temperature. *Nano Lett.* **13**, 4532–4538, doi:10.1021/nl402513x (2013).
- Liu, J. P. *et al.* Co_3O_4 nanowire/ MnO_2 ultrathin nanosheet core/shell arrays: a new class of high-performance pseudocapacitive materials. *Adv. Mater.* **23**, 2076–2081, doi:10.1002/adma.v23.18 (2011).
- Zhang, L. L. & Zhao, X. S. Carbon-based materials as supercapacitor electrodes. *Chem. Soc. Rev.* **38**, 2520–2531, doi:10.1039/b813846j (2009).
- Wang, Z. L., Zhu, Z. L., Qiu, J. H. & Yang, S. H. High performance flexible solid-state asymmetric supercapacitors from MnO_2/ZnO core-shell nanorods/specially reduced graphene oxide. *J. Mater. Chem. C* **2**, 1331–1336, doi:10.1039/C3TC31476F (2014).
- Simon, P., Gogotsi, Y. & Dunn, B. Where do batteries end and supercapacitors begin? *Science* **343**, 1210–1211, doi:10.1126/science.1249625 (2014).
- Wang, G. P., Zhang, L. & Zhang, J. J. A review of electrode for electrochemical supercapacitors. *Chem. Soc. Rev.* **41**, 797–828, doi:10.1039/C1CS15060J (2012).
- Yuan, C. Z., Wu, H. B., Xie, Y. & Lou, X. W. Mixed transition-metal oxides: design, synthesis, and energy-related applications. *Angew. Chem. Int. Ed.* **53**, 1488–1504, doi:10.1002/anie.201303971 (2014).
- Wang, X. W. *et al.* Co_3O_4 @MWCNT nanocable as cathode with superior electrochemical performance for supercapacitors. *ACS App. Mater. Interfaces* **7**, 2280–2285, doi:10.1021/am5062272 (2015).
- Wang, Y. P. *et al.* Facile synthesis of nanorod-assembled multi-shelled Co_3O_4 hollow microspheres for high-performance supercapacitors. *J. Power Sources* **272**, 107–112, doi:10.1016/j.jpowsour.2014.08.067 (2014).

21. Wang, Y., Zhong, Z. Y., Chen, Y., Ng, C. T. & Lin, J. Y. Controllable synthesis of Co_3O_4 from nanosize to microsize with large-scale exposure of active crystal planes and their excellent rate capability in supercapacitors based on the crystal plane effect. *Nano Res* **4**, 695–704, doi:10.1007/s12274-011-0125-x (2011).
22. Yan, J. *et al.* Advanced asymmetric supercapacitors based on $\text{Ni}(\text{OH})_2/\text{graphene}$ and porous graphene electrodes with high energy density. *Adv. Funct. Mater.* **22**, 2632–2641, doi:10.1002/adfm.201102839 (2012).
23. Qu, L. B. *et al.* Interwoven three-dimensional architecture of cobalt oxide nanobrush-graphene@ $\text{Ni}_x\text{Co}_{2x}(\text{OH})_{6x}$ for high performance supercapacitors. *Nano Lett.* **15**, 2037–2044, doi:10.1021/nl504901p (2015).
24. Hosono, E., Fujihara, S., Honma, I., Ichihara, M. & Zhou, H. Synthesis of the CoOOH fine nanoflake film with the high rate capacitance property. *J. Power Sources* **158**, 779–785, doi:10.1016/j.jpowsour.2005.09.052 (2006).
25. Yuan, C. Z., Zhang, X. G., Gao, B. & Li, J. Synthesis and electrochemical capacitance of mesoporous $\text{Co}(\text{OH})_2$. *Mater. Chem. Phys.* **101**, 148–152, doi:10.1039/c0nr00423e (2007).
26. Gupta, V., Kusahara, T., Toyama, H., Gupta, S. & Miura, N. Potentiostatically deposited nanostructured $\alpha\text{-Co}(\text{OH})_2$: A high performance electrode material for redox-capacitors. *Electrochem. Commun.* **9**, 2315–2319, doi:10.1016/j.elecom.2007.06.041 (2007).
27. Wang, Y. F. *et al.* ZIF-8@MWCNT derived carbon composite as electrode of high performance for supercapacitor. *Electrochim. Acta* **213**, 260–269, doi:10.1016/j.electacta.2016.07.019 (2016).
28. Zhu, L., Wu, W. Y., Zhu, Y. S., Tang, W. P. & Wu, Y. P. Composite of CoOOH Nanoplates with Multiwalled Carbon Nanotubes as Superior Cathode Material for Supercapacitors. *J. Phys. Chem. C* **119**, 7069–7075, doi:10.1021/acs.jpcc.5b01498 (2015).
29. Cheng, F. Y. *et al.* Porous LiMn_2O_4 nanorods with durable high-rate capability for rechargeable Li-ion batteries. *Energy Environ. Sci.* **4**, 3668–3575, doi:10.1039/c1ee01795k (2011).
30. Lin, H. B. *et al.* Porous LiMn_2O_4 cubes architected with single-crystalline nanoparticles and exhibiting excellent cyclic stability and rate capability as the cathode of a lithium ion battery. *J. Mater. Chem. A* **2**, 9272–9279, doi:10.1039/c4ta01474j (2014).

Acknowledgements

Financial supports from National Materials Genome Project (2016YFB0700600), Natural Distinguished Youth Scientists Project of China (No. 51425301), National Science Foundation Committee of China (21374021 and U1601214), Science and Technology Commission of Shanghai Municipality (12JC1401200 and 14520721800) and Sanyo Chemical Co. Ltd. are greatly appreciated.

Author Contributions

Y.W. designed this Faradaic capacitor. Y.W. and Z.C. carried out the electrochemical experiments and other analyses. Y.W., Z.C., Y.Z. and B.C. analyzed and discussed the results and wrote the manuscript. L.F., Y.Z., L.Z., and Y. Wu. supervised the research project.

Additional Information

Supplementary information accompanies this paper at doi:10.1038/s41598-017-02004-8

Competing Interests: The authors declare that they have no competing interests.

Publisher's note: Springer Nature remains neutral with regard to jurisdictional claims in published maps and institutional affiliations.



Open Access This article is licensed under a Creative Commons Attribution 4.0 International License, which permits use, sharing, adaptation, distribution and reproduction in any medium or format, as long as you give appropriate credit to the original author(s) and the source, provide a link to the Creative Commons license, and indicate if changes were made. The images or other third party material in this article are included in the article's Creative Commons license, unless indicated otherwise in a credit line to the material. If material is not included in the article's Creative Commons license and your intended use is not permitted by statutory regulation or exceeds the permitted use, you will need to obtain permission directly from the copyright holder. To view a copy of this license, visit <http://creativecommons.org/licenses/by/4.0/>.

© The Author(s) 2017